AGU PUBLICATIONS

JGR

Journal of Geophysical Research: Biogeosciences

RESEARCH ARTICLE
10.1002/2016JG003331

Key Points:
- Typhoon Damrey increased the phytoplankton biomass in both the surface and subsurface layers
- Phytoplankton biomass experienced different changing processes in the two layers
- Contributions of physical and biogeochemical processes were different in the two layers

Correspondence to:
J. Shi,
shijie@ouc.edu.cn

Citation:
Pan, S., J. Shi, H. Gao, X. Guo, X. Yao, and X. Gong (2017), Contributions of physical and biogeochemical processes to phytoplankton biomass enhancement in the surface and subsurface layers during the passage of Typhoon Damrey, *J. Geophys. Res. Biogeosci.*, *122*, 212–229, doi:10.1002/2016JG003331.

Received 11 JAN 2016
Accepted 4 JAN 2017
Accepted article online 9 JAN 2017
Published online 25 JAN 2017

Contributions of physical and biogeochemical processes to phytoplankton biomass enhancement in the surface and subsurface layers during the passage of Typhoon Damrey

Shanshan Pan[1,2], Jie Shi[1,2], Huiwang Gao[1,2], Xinyu Guo[1,2,3], Xiaohong Yao[1,2], and Xiang Gong[1,2]

[1]Key Laboratory of Marine Environment and Ecology, Ministry of Education, Qingdao, China, [2]College of Environmental Science and Engineering, Ocean University of China, Qingdao, China, [3]Center for Marine Environmental Studies, Ehime University, Matsuyama, Japan

Abstract In this study, a one-dimensional physical-biogeochemical coupled model was established to investigate the responses of the upper ocean to Typhoon Damrey in the basin area of the South China Sea. The surface chlorophyll *a* concentration (Chl *a*) increased rapidly from 0.07 to 0.17 mg m^{-3} when the typhoon arrived and then gradually reached a peak of 0.61 mg m^{-3} after the typhoon's passage. The subsurface Chl *a* decreased from 0.34 to 0.17 mg m^{-3} as the typhoon arrived and then increased gradually to 0.71 mg m^{-3}. Analyses of model results indicated that the initial rapid increase in the surface Chl *a* and the decrease in the subsurface Chl *a* were caused mainly by physical process (vertical mixing), whereas the subsequent gradual increases in the Chl *a* in both the surface and subsurface layers were due mainly to biogeochemical processes (net growth of phytoplankton). The gradual increase in the Chl *a* lasted for longer in the subsurface layer than in the surface layer. Typhoon Damrey yielded an integrated primary production (IPP) of 6.5×10^3 mg C m^{-2} (~14% of the annual IPP in this region).

1. Introduction

Typhoons are intense atmospheric events with strong effects on the physical and biogeochemical processes in oceans [*Tang et al.*, 2014; *Guan et al.*, 2014; *Yang et al.*, 2015]. Many studies have suggested that typhoons can enhance the chlorophyll *a* concentration (Chl *a*) in the upper water layer, as well as causing phytoplankton blooms via nutrient pumping to the surface [*Zheng and Tang*, 2007; *Shan et al.*, 2014; *Zhao et al.*, 2015]. Consequently, typhoons can promote marine primary production and associated carbon fixation [*Lin et al.*, 2003; *Sun et al.*, 2010]. Moreover, typhoons can strengthen ocean-atmosphere CO_2 exchange and hence year-to-year variability of CO_2 fluxes over the subtropical oceans [*Bates et al.*, 1998]. However, due to the rough sea conditions associated with typhoon events, only a few shipboard observations are available to study typhoons and their oceanic impacts [*Zheng and Tang*, 2007; *Zhao et al.*, 2009; *Ye et al.*, 2013]. In addition, observations collected by moorings during typhoon events can only be captured by chance [*Dickey et al.*, 1998; *Zedler et al.*, 2002; *Guan et al.*, 2014; *Yang et al.*, 2015]. Thus, the responses of Chl *a* have been analyzed mainly at the surface based on satellite data [*Babin et al.*, 2004; *Tang et al.*, 2004a; *Walker et al.*, 2005; *Zhao et al.*, 2008; *Zhao et al.*, 2013].

Typhoon Kai-Tak passed over the South China Sea (SCS) and triggered a 30-fold increase in the surface Chl *a* in July 2000 [*Lin et al.*, 2003]. In the central Arabian Sea, the surface Chl *a* increased from ~0.4 mg m^{-3} up to 4 mg m^{-3} over a large area due to a moderate tropical cyclone in December 1998 [*Naik et al.*, 2008]. The Chl *a* increased more than 20-fold after the passage of typhoon Hagibis in the middle of the SCS in November 2007 [*Sun et al.*, 2010]. Satellite data indicate that a significant increase of Chl *a* by 0.8 mg m^{-3} was associated with hurricane Igor over the adjacent Grand Banks of Newfoundland in September 2010 [*Han et al.*, 2012]. The fast-moving and weak tropical storm Washi enhanced the surface Chl *a* by ~20% over the continental shelf southeast of the SCS in July 2005 [*Zhang et al.*, 2014]. The contributions of typhoons to ocean primary production have also been estimated based on satellite data. Typhoon Kai-Tak contributed 2–4% of the annual primary production in the SCS [*Lin et al.*, 2003]; Typhoon Hagibis contributed up to 30% [*Sun et al.*, 2010].

Subsurface chlorophyll *a* maximum (SCM) has been observed frequently in tropical and subtropical oceans throughout the whole year, while it occurs during the warm season in temperate ocean zones. The subsurface layer has been reported to be the most productive layer among the whole water column in tropical and subtropical oceans throughout the year and in temperate ocean zones during summer [*Gong et al*., 2000; *Liu et al*., 2002; *Ardyna et al*., 2013; *Gong et al*., 2015]. However, satellite data can only indicate the distribution of Chl *a* in the surface layer. Thus, little information has been documented about the responses of the subsurface Chl *a* to typhoons and the mechanisms involved. Field observations conducted 10 days after typhoon. Observations conducted ten days after the typhoon Nuri in 2008 showed that there was also a phytoplankton bloom in the subsurface layer following the surface bloom [*Ye et al*., 2013]. It is likely that the subsurface phytoplankton bloom induced by typhoons may be different from that in the surface layer in terms of its duration and magnitude.

The mechanisms involved in the impacts of typhoons on phytoplankton blooms and primary production may change with region and depth. Strong vertical mixing, upwelling, and even high rainfall are induced by typhoons [*Tang et al*., 2014]. For example, Typhoon Damrey, which occurred in the SCS during September 2005, triggered an offshore surface phytoplankton bloom due to increased nutrient levels as a result of vertical mixing and upwelling, and a nearshore bloom because of rainwater discharge and seaward advection by a typhoon-induced current [*Zheng and Tang*, 2007]. *Zhao et al*. [2015] found that the low Chl *a* in the offshore area increased supported by the addition of nutrients by upwelling and vertical mixing. Usually, vertical mixing is suggested to be the primary mechanism for cooling the ocean below the typhoons [*Price*, 1981; *Knaff et al*., 2013]. The vertical mixing is typically 10 times more effective at cooling the upper ocean than the wind-driven upwelling [*Jacob et al*., 2000; *Cione and Uhlhorn*, 2003]. The lasting time of upwelling is typically half a day, which is shorter than that of vertical mixing, whose effects last for 5–10 days [*Price et al*., 1994].

Satellite-based and shipboard data have demonstrated that typhoon-induced vertical mixing can enhance the surface Chl *a*. One cause of the rapid growth of surface phytoplankton is the biogeochemical response to the supply of nutrients from deep layers. Another cause is the physical entrainment of phytoplankton from the subsurface layer where the SCM is formed. However, it is unclear whether the observed increase in Chl *a* is due to the supply of nutrients or the physical entertainment of phytoplankton from the subsurface, or both processes [*Walker et al*., 2005; *Ye et al*., 2013]. Moreover, it is logistically difficult and expensive to quantify the contributions of these two processes to the change of surface Chl *a* by only observations. *Shibano et al*. [2011] showed that without biogeochemical processes, the increase in Chl *a* in a numerical model was much smaller than observation, indicating that the biogeochemical processes are essential factors related to surface phytoplankton increases. However, they did not quantify the contributions of physical and biogeochemical processes to the increases in the surface phytoplankton.

The SCS is the largest marginal sea in the western Pacific (Figure 1), with an average depth of 1200 m and a total area of $\sim 3.5 \times 10^6$ km^2 [*Wang et al*., 2009; *Yang et al*., 2002]. The upper water is permanently stratified and oligotrophic in the basin area due to strong solar radiation throughout the year. In addition, a significant phytoplankton biomass is generally observed in the subsurface, which is the most productive layer [*Gong et al*., 2000; *Liu et al*., 2002; *Gong et al*., 2015]. The primary production depends mainly on the supply of nutrients from deeper nutrient-rich water to the euphotic zone by turbulent vertical transport [*Tang et al*., 2004b]. The SCS is located in an area with a high frequency of tropical cyclones [*Ha et al*., 2014; *Li and Zhou*, 2014] and more than 10 typhoons pass through this region each year [*Wang et al*., 2007].

In order to quantify the contribution of vertical mixing strengthened by Typhoon Damrey in 2005 to the enhancement of phytoplankton biomass, a one-dimensional (1-D) vertically resolved physical-biogeochemical coupled model was established in the stratified basin area of the SCS. After describing the responses of the vertical profiles of temperature, nutrients, and Chl *a*, the contributions of physical and biogeochemical processes to the changes of phytoplankton biomass in different water layers were quantified. Moreover, the contributions of Typhoon Damrey to the vertical transport of nutrients and ocean primary production were calculated and compared with other studies. The potential long-term impacts of typhoons were also discussed.

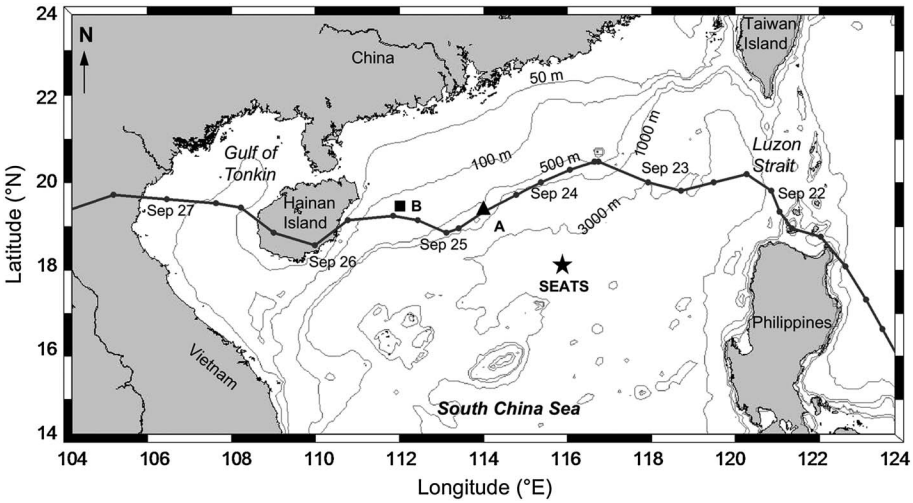

Figure 1. Topography of the northern South China Sea and the track of Typhoon Damrey. The locations of SEATS (18°N, 116°E), Station A (19.3°N, 114°E), and Station B (19°35′N, 112°E) are denoted by the star, triangle, and rectangle, respectively. The center position of the typhoon every 6 h is indicated by gray points. The dates beside the typhoon center were at 00:00 h on each day. All dates and times are in universal time coordinated.

2. Methods

2.1. Model Description

The 1-D model comprises a hydrodynamic module and a biogeochemical module. The hydrodynamic module provides the water temperature and diffusivity coefficient to the biogeochemical module.

The hydrodynamic module is based on the 1-D Princeton Ocean Model [*Blumberg and Mellor*, 1987]. The embedded level-2.5 Mellor-Yamada turbulent closure model is used to calculate the vertical viscosity and diffusivity. However, the calculated mixed layer is always warmer and shallower than observations [*Martin*, 1985]. To address this problem, turbulent mixing is amplified by considering the effects of waves [*Zhang*, 2003; *Hu et al*., 2004; *Huang and Qiao*, 2010; *Huang et al*., 2011]. In our model, we use a simple parameterized scheme based on the descriptions given by *Hu et al*. [2004] and *Zhang* [2003]. The surface wave-induced vertical kinematic viscosity (K_{wm}) and diffusivity (K_{wh}) are added to those calculated by the Mellor-Yamada turbulent closure model. K_{wm} and K_{wh} are given by

$$K_{wm} = \frac{2k^2}{g}\delta\beta^3 W^3 e\frac{gz}{\beta^2 W^2}, \tag{1}$$

$$K_{wh} = PK_{wm}, \tag{2}$$

where $k = 0.4$ is von Karman's constant, $g = 9.8\,\mathrm{m\,s^{-2}}$ is the gravitational acceleration, $\delta = 0.1$ is the wave steepness, $\beta = \frac{c}{W} < 1.0$ is the wave age, c is the wave velocity ($\mathrm{m\,s^{-1}}$), W is the surface wind speed ($\mathrm{m\,s^{-1}}$), z is the vertical coordinate positive upward (m), and P is a dimensionless coefficient related to the Richardson number, where $P = 0.1$ [*Hu et al*., 2004; *Zhang*, 2003].

The biogeochemical module is simplified from the biomass-based European Regional Sea Ecosystem Model [*Baretta et al*., 1995; *Vichi et al*., 2004]. As shown in Figure 2, 10 state variables are included: three nutrient elements (dissolved inorganic nitrogen (DIN), dissolved inorganic phosphate (DIP), and dissolved silicate (DSi)), phytoplankton, bacterioplankton, three related types of zooplankton (mesozooplankton, microzooplankton, and heterotrophic nanoflagellates), and organic matter (in dissolved form (DOM) and particle form (detritus)). Phytoplankton absorbs nutrients for photosynthesis, and it is consumed by mesozooplankton and microzooplankton. Bacterioplankton feeds on organic matter (DOM and detritus), and it is grazed by heterotrophic nanoflagellates. Mesozooplankton is at the highest trophic level in the model, and it feeds on phytoplankton and microzooplankton. DOM is produced by the excretion of phytoplankton, bacterioplankton, microzooplankton, and heterotrophic nanoflagellates. Detritus is produced by the fecal pellets of zooplankton and the dead remains of phytoplankton and zooplankton. DIP and DIN are recycled from DOM and detritus,

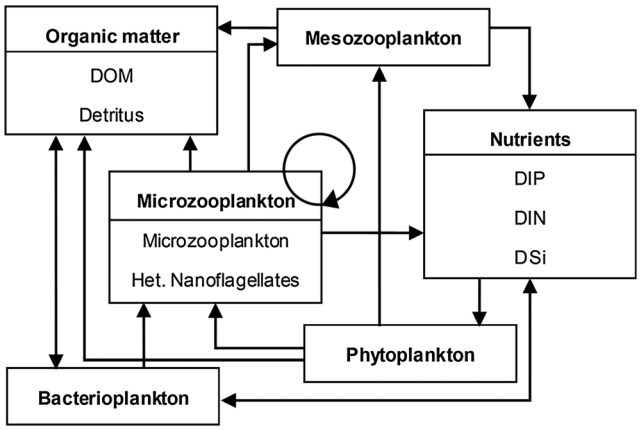

Figure 2. Schematic view of the biogeochemical module.

whereas DSi is released only from detritus. The parameters used in the model are based on those reported in previous studies, and they are listed in Tables 1 and 2.

2.2. Model Configuration and Data Sources

The water depth in the model is set to 1200 m, which is the average depth of the SCS, thereby representing the permanent stratified basin area. There are 40 layers in the vertical direction. In the basin area of the SCS, the seasonal variation and responses to typhoons occur mainly in the upper layers [*Tseng et al*., 2005]. Thus, there are 35 layers in the upper 150 m depth and five layers below 150 m depth in our model. Both the physical and biological variables are calculated simultaneously at a time step of 216 s.

The model is forced by wind and heat fluxes. The air-sea net heat flux has four components. Net longwave radiation flux and net short wave radiation flux were derived from National Centers for Environmental Prediction (NCEP) reanalysis data sets (http://www.esrl.noaa.gov/psd/data/gridded/reanalysis/). Sensible heat flux and latent heat flux are calculated by using the COARE 2.0 bulk flux algorithm [*Fairall et al*., 1996] based on the air temperature, sea surface temperature (SST), relative humidity, air pressure, and wind speed. The sea surface salinity (SSS) was also derived from NCEP reanalysis data sets.

The numerical simulations comprised two cases, which we refer to as CONTROL and TYPHOON. In CONTROL, we simulated climatological seasonal cycles in the ecosystem at the South East Asia Time Series Study (SEATS) station (18°N, 116°E) (Figure 1). Wind forcing, SSS, net longwave radiation flux, and net short wave radiation flux were obtained from NCEP monthly long-term mean data collected between 1981 and 2010 at the SEATS

Table 1. General Parameters in the Model and Their Sensitivities

Parameter	Symbol	Value	Sensitivity
Fraction of photosynthetically available radiation (–)	$\varepsilon_{\mathrm{PAR}}$	0.40	
Optical extinction coefficient for pure water (m^{-1})	λ_W	0.06	
Optical extinction coefficient for phytoplankton (m^{-1} (mg C m^{-3})$^{-1}$)	λ_{phyt}	0.5×10^{-3}	0.00
Settling velocity of particulate detritus (m d^{-1})	v_{R6}^{sed}	1.00	0.22
Parameters of Phytoplankton			
Maximum specific photosynthetic rate (per day)	r_{0p}	2.60	0.93
Characteristic Q_{10} coefficient	Q_{10p}	2.00	0.94
Half saturation value for N limitation (mmol N m^{-3})	h_p^n	0.50	0.85
Half saturation value for P limitation (mmol P m^{-3})	h_p^p	0.05	0.27
Half saturation value for Si limitation (mmol Si m^{-3})	h_p^s	0.30	0.00
Basal specific respiration rate (per day)	b_p	0.01	0.44
Activity respiration fraction (–)	γ_p	0.10	0.04
Excreted fraction of primary production (–)	β_p	0.05	0.62
Maximum specific lysis rate (per day)	d_{0p}	0.50	0.19
Standard Si:C ratio in diatoms (mmol Si mg C^{-1})	$s_{p^{(1)}}^{\mathrm{opt}}$	0.01	0.49
Optimal C:chl quota (mg C mg chl^{-1})	θ_{chl}^0	25.00	0.00
Parameters for Bacterioplankton			
Potential specific growth rate (per day)	r_{0B}	8.38	0.00
Basal specific respiration rate (per day)	b_B	0.01	0.09
Assimilation efficiency (–)	η_B	0.40	0.41
Specific mortality rate (per day)	d_{0_B}	0.00	0.09
Specific potential $R^{(1)}$ uptake (per day)	v_B^1	0.30	0.32
Specific potential $R^{(6)}$ uptake (per day)	v_B^6	0.01	0.22
Specific rate of uptake or remineralization (per day)	$v_B^n = v_B^p$	1.00	0.14

Table 2. Parameters for the Zooplankton Groups and Their Sensitivities

		Mesozooplankton		Microzooplankton		Heterotrophic Nanoflagellates	
Parameter	Symbol	Value	Sensitivity	Value	Sensitivity	Value	Sensitivity
Characteristic Q_{10} coefficient (per day)	Q_{10z}	3.00	0.06	2.00	0.96	2.00	0.16
Michaelis constant for total food ingestion (mg C m^{-3})	h_z^F	80.00	0.09	20.00	0.32	20.00	0.06
Feeding threshold (mg C m^{-3})	μ_z	0.00		20.00	0.14	20.00	0.04
Potential specific growth rate (per day)	r_{0z}	2.00	0.00	2.00	0.83	10.00	0.08
Basal specific respiration rate (per day)	b_z	0.02	0.03	0.02	0.12	0.02	0.07
Assimilation efficiency (−)	η_z	0.60	0.00	0.60	0.75	0.50	0.24
Excreted fraction of uptake (−)	β_z	0.55	0.02	0.40	0.14	0.30	0.45
Partition between dissolved and particulate excretion of C (−)	ε_z^c	0.00		0.50	0.37	1.00	0.09
Partition between dissolved and particulate excretion of N (−)	ε_z^n	0.00		0.84	0.24	1.00	0.10
Partition between dissolved and particulate excretion of P (−)	ε_z^p	0.00		0.96	0.04	1.00	0.03
Specific rate of nutrients and carbon excretion (per day)	v_z	1.00	0.01	1.00	0.05	1.00	0.02
Specific mortality rate (per day)	d_{0z}	0.02	0.00	0.05	0.03	0.05	0.01
Density-dependent specific mortality rate (m^3 mg C^{-1} d^{-1})	d_z^{dns}	0.02	0.01	0.00		0.00	
Exponent for density dependent mortality (−)	γ_z	2.50	0.04				

station. The model was initialized with the multiyear averaged vertical profiles of the water temperature, salinity, nutrient concentrations, and Chl *a* observed at the SEATS station in winter. The initial concentrations of bacterioplankton, zooplankton, and organic matter (DOM and detritus) were set to zero. The coupled model was integrated for 3 years under the same surface climatological forcing to obtain a quasi-steady state. The results of the third year were used to compare with observations collected at the SEATS station and the World Ocean Atlas 2013 (WOA2013) statistical mean data (http://www.nodc.noaa.gov/OC5/woa13/woa13-data.html) interpolated to the SEATS station in four seasons. The observed temperature, salinity, and Chl *a* at the SEATS station were reported by *Chen* [2004] and *Liu et al*. [2007], and the observed temperature, salinity, Chl *a*, and nutrients were the unpublished data provided by Prof. Minhan Dai from Xiamen University of China (personal communication). The specific information of the observations used for model validations was listed in Table 3. The observations at the SEATS station as reported by *Liu et al*. [2013] were also used for comparison with the modeled surface Chl *a*.

In TYPHOON, the model was initialized with the results obtained by CONTROL for 20 September, which was the day before the arrival of Typhoon Damrey. Surface forcing data, including the wind and heat flux during typhoon period from 20 to 30 September 2005, were obtained from NCEP data collected at 6 h intervals near Station A (19.3°N, 114°E) (Figure 1). The exact wind speed was not available at Station A, and thus, the wind speed determined from the NCEP reanalysis was used for forcing. The coupled 1-D model was integrated from 20 September until the end of the year. The simulated vertical profile of the water temperature before the arrival of Typhoon Damrey on 20 September was also compared with shipboard observations collected at Station A [*Zheng and Tang*, 2007]. Typhoon Damrey happened to pass by a mooring station (19°35′N, 112°E) (Station B in Figure 1) on the continental shelf of the northwestern SCS. The observed variation of temperature caused by the Typhoon Damrey [*Yang et al*., 2015] was used to compare with and validate the model results. The daily SST and sea surface Chl *a* time series during the passage of the typhoon were validated by using daily Tropical Rainfall Measuring Mission (TRMM) Microwave Imager (TMI) SST data (http://www.remss.com/) and Chl *a* values derived from the Moderate Resolution Imaging Spectroradiometer (MODIS)

Table 3. Information of Observations at the SEATS Station Used for Model Validations

	Observations				
Variables	Winter	Spring	Summer	Autumn	Data Source
Temperature, salinity, and Chl *a*	Jan 2003	May 2000	Jul 2000	Nov 1999	Observations1[a]
	Jan 2010	May 2011	Aug 2009 and 2012	Nov 2006 and 2010	Observations2[b]
Nutrients	Feb	May	Aug	Nov	WOA2013
	Jan 2010	May 2011	Aug 2009 and 2012	Nov 2006 and 2010	Observations2

[a]Observations1 was the data from *Chen* [2004] and *Liu et al*. [2007].
[b]Observations2 was the unpublished data from Prof. Minhan Dai (personal communication).

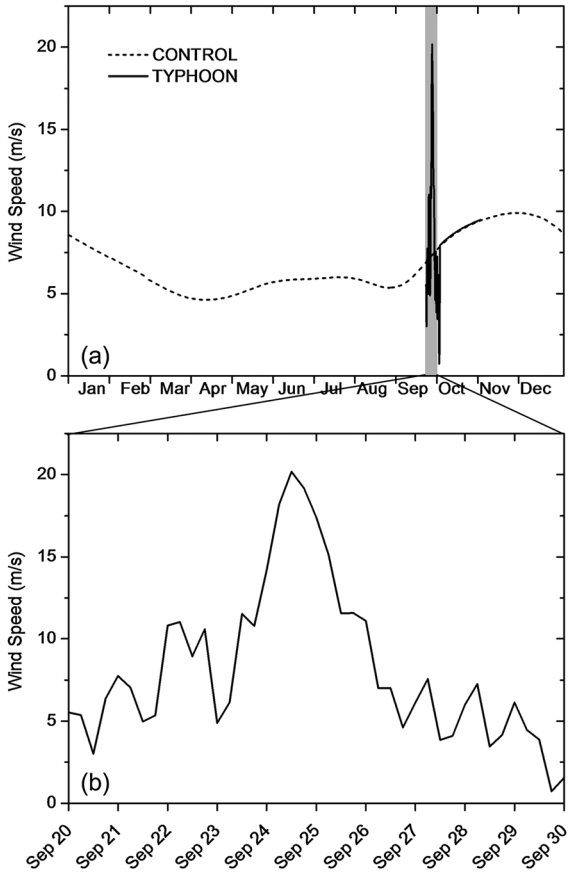

Figure 3. (a) Time series of wind speed (m/s) from NCEP for the CONTROL (dash line) and TYPHOON (solid line) simulations. For CONTROL simulation, the wind speed was obtained from NCEP monthly long-term mean (1981 to 2010) data collected at the South East Asia Time Series Study (SEATS) station (18°N, 116°E). (b) For TYPHOON simulation, the wind speed from 20 to 30 September 2005 comprised 6 h interval data from Station A (19.3°N, 114°E), which were obtained from NCEP.

onboard Aqua (http://oceandata.sci.gsfc.nasa.gov/MODISa/Mapped/Daily/9 km/) and Sea-viewing Wide Field-of-view Sensor (SeaWiFS) (http://oceandata.sci.gsfc.nasa.gov/SeaWiFS/Mapped/Daily/9km/), respectively.

Typhoon tracking data are issued by the Japan Meteorological Agency, and they were obtained from the Typhoon Database of the National Institute of Informatics of Japan (http://agora.ex.nii.ac.jp), including the center location, central pressure, and maximum 10 min sustained wind speeds every 6 h. The satellite-derived images of SST and sea surface Chl *a* before, during, and after Typhoon Damrey were from the daily TMI data with spatial resolution of 0.25° and MODIS standard level2 products with spatial resolution of 1 km, respectively.

3. Results

3.1. Modeled Climatological Seasonal Trends of the Upper Ocean Ecosystem

The seasonal variations in physical and biological variables in the upper layer of the SCS are controlled primarily by the East Asian monsoon [*Wong et al.*, 2007; *Liu et al.*, 2013]. The NCEP reanalysis data sets showed that the wind speed in our study area was approximately 5 m s^{-1} in the summer monsoon season (from June to September), before increasing up to approximately 10 m s^{-1} in the winter monsoon season from November to March, and it was approximately 4 m s^{-1} during spring and fall (Figure 3a).

The modeled results in February, May, August, and November represented results in winter, spring, summer, and autumn. The modeled vertical profiles of physical variables were in good agreement with the observations collected at the SEATS station (Figure 4). The East Asian monsoon also affected the vertical structure of the water temperature and salinity in the study area by wind forcing (Figures 4a and 4b). According to the modeled results, the SST reached its highest value of 29.5°C in summer and a lowest value of 23.6°C in winter. SSS varied from 33.09 to 34.10 with two lowest salinity periods in May and October. In this study, we defined the mixed layer depth (MLD) as the depth where the water temperature is 1°C lower than the mean value of the surface layer in the 10 m depth [*Wagner*, 1997] (Figure 4a). The calculated MLD was over 90 m in the winter monsoon season, which was the largest among the four seasons because of the high wind speed and strong water surface cooling. In spring, the calculated MLD became shallower due to enhanced solar radiation and weakening of the wind speed. As the solar radiation increased further in the summer monsoon season, the calculated MLD was approximately 20 m. The calculated MLD gradually deepened during fall as the winter monsoon formed. The calculated vertical diffusivity coefficient in the upper ocean (Figure 4c) varied seasonally, and it was closely related to the wind speed. In the winter monsoon season,

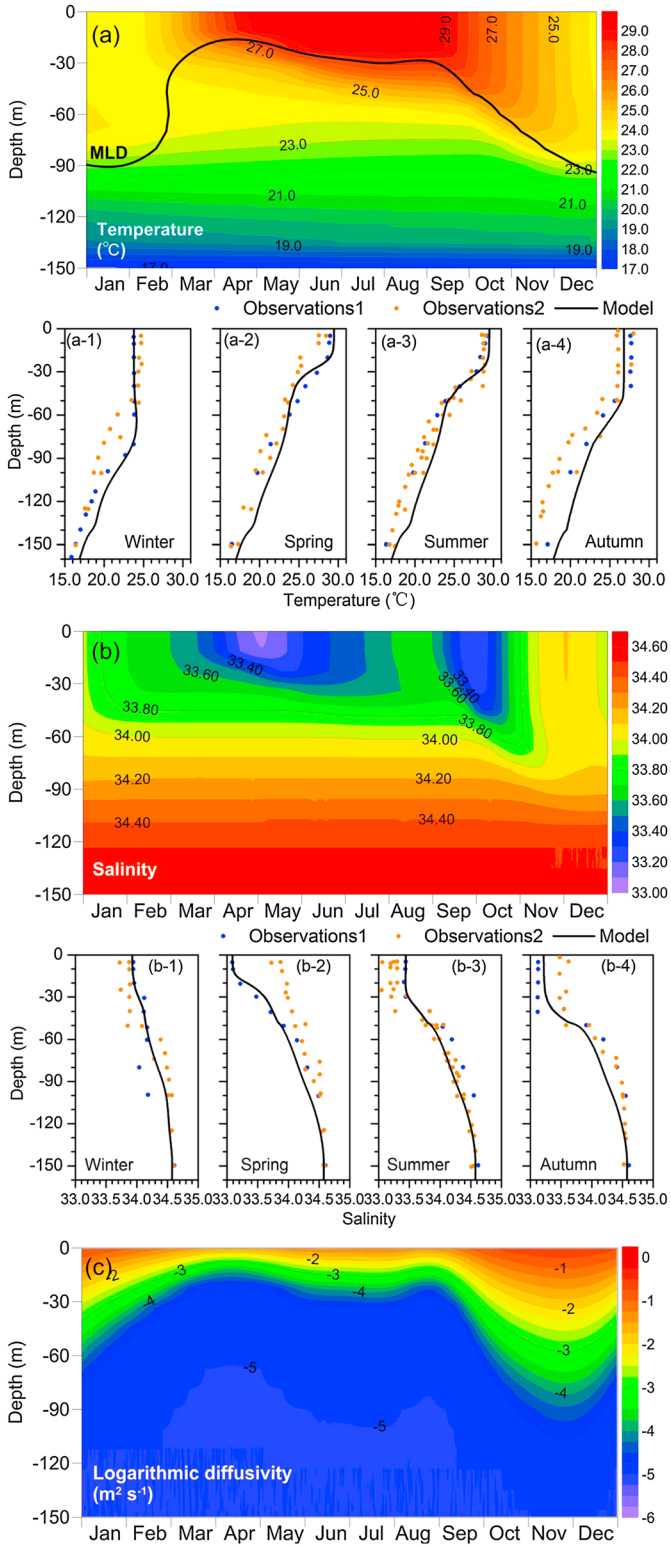

Figure 4. Depth-time plots of the modeled (a) water temperature (°C), (b) salinity, and (c) logarithmic distributions of the vertical diffusivity coefficient ($m^2 s^{-1}$) in the CONTROL simulation, where the thick solid line in Figure 4a represents the mixed layer depth (MLD, unit: meter). Modeled vertical profiles of the water temperature (a-1 to a-4) and salinity (b-1 to b-4) in four seasons are plotted to compare with the observations acquired at the SEATS station. Observations1 (denoted by blue dots) is reported by *Chen* [2004] and *Liu et al.* [2007]. Observations2 (denoted by orange dots) is the unpublished data provided by Prof. Minhan Dai from Xiamen University of China.

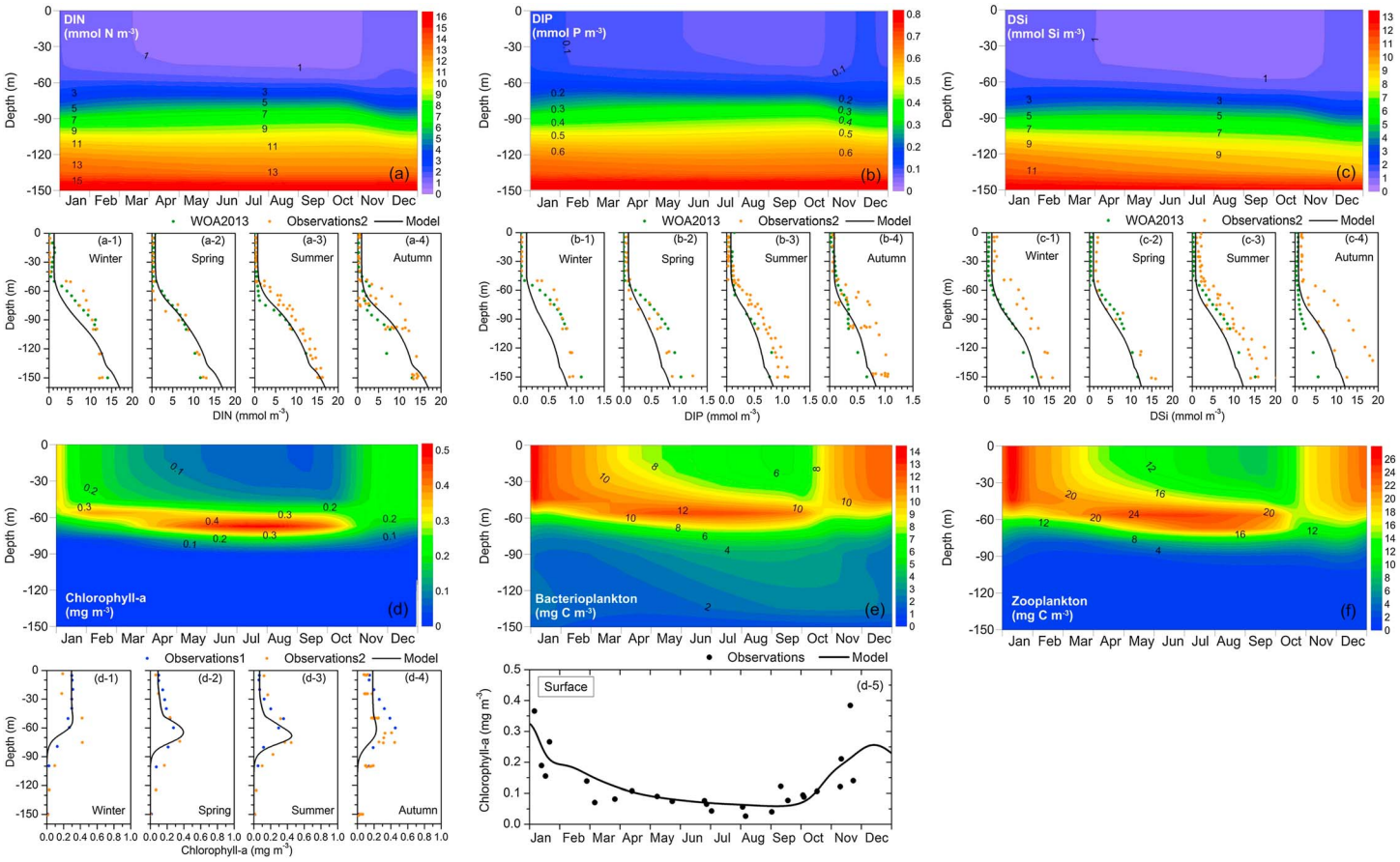

Figure 5. Depth-time plots of the modeled (a) dissolved inorganic nitrogen (DIN, unit: mmol m^{-3}), (b) dissolved inorganic phosphate (DIP, unit: mmol m^{-3}), (c) dissolved silicate (DSi, unit: mmol m^{-3}), (d) Chl *a* (mg m^{-3}), (e) bacterioplankton (mg C m^{-3}), and (f) zooplankton (mg C m^{-3}) in the CONTROL simulation. Modeled vertical profiles of the DIP (a-1 to a-4), DIN (b-1 to b-4), DSi (c-1 to c-4), and Chl *a* (d-1 to d-4) in four seasons are plotted to compare with observations at SEATS station. Observations1 (denoted by blue dots) is reported by *Chen* [2004] and *Liu et al.* [2007]. Observations2 (denoted by orange dots) is the unpublished data provided by Prof. Minhan Dai from Xiamen University of China. The green dots are from WOA2013. The black dots in Figure 5d-5 are from *Liu et al.* [2013].

the calculated vertical diffusivity coefficient was 10^{-1} m^2 s^{-1} at the surface and it decreased to 10^{-4} m^2 s^{-1} at the 80 m depth, thereby corresponding to the strong winter monsoon. In the summer monsoon season, the calculated vertical diffusivity coefficient was 10^{-2} m^2 s^{-1} at the surface and less than 10^{-4} m^2 s^{-1} below the 30 m depth. The vertical diffusivity coefficient decreased downward throughout the year.

Changes in physical variables such as the wind and water temperature can influence the vertical profiles of biological elements and their seasonal variations. The modeled DIP, DIN, and DSi values were approximately within the ranges of multiyear observations at the SEATS station, and the vertical structures were in good agreement with observations (Figures 5a–5c). The calculated nutrient elements (DIN, DIP, and DSi) exhibited only slight seasonal variations. In this study, the depth of the nitracline was defined as the depth where the nitrate concentration was 1 mmol m^{-3} [*Cullen and Eppley*, 1981; *Raimbault et al.*, 1993]. According to this threshold, the depth of the nitracline was located at a depth of about 50 m, which was deeper than the MLD throughout the whole year, except in the winter. Physical stratification acts as a physical barrier that prevents the upward transport of nutrients from deeper nutrient-rich water below the depth of the nutricline. As a result, the nutrient concentrations are low in the upper 50 m depth in the warm season, which are deficient for the growth of phytoplankton [*Fisher*, 1992]. In the winter monsoon season, the modeled DIN, DIP, and DSi concentrations at the surface reached maximum values of 1.4 mmol m^{-3}, 0.11 mmol m^{-3}, and 1.4 mmol m^{-3}, respectively, because of the enhanced vertical mixing.

The model reproduced the seasonal variations of Chl *a* observed at the SEATS station (Figure 5d). Modeled results showed that the sea surface Chl *a* varied from 0.06 to 0.32 mg m^{-3} with a prominent peak in winter.

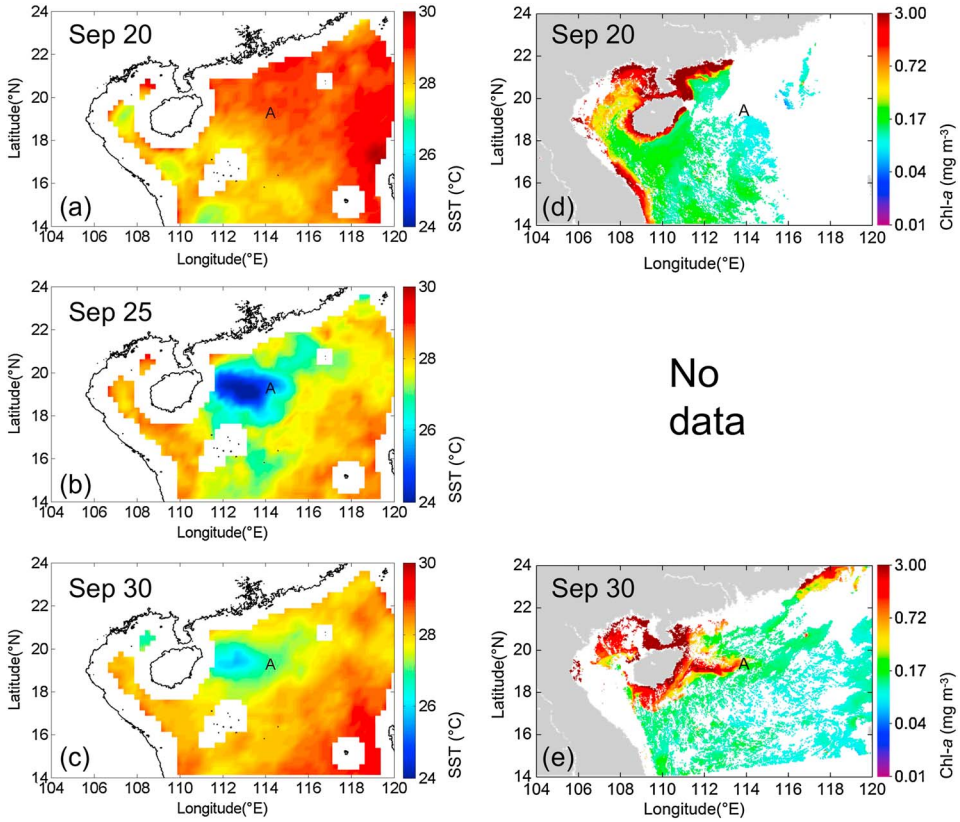

Figure 6. (a–c) Sea surface cooling and (d and e) Chl *a* increase related to Typhoon Damrey. The daily SST and sea surface Chl *a* on 20, 25, and 30 September 2005 are retrieved from TMI and MODIS-Aqua, respectively.

Excluding the winter monsoon season, the calculated SCM was identified at a depth of approximately 60 m, which was located immediately below the depth of the nutricline and above the euphotic layer depth (defined as the depth with 1% of the surface solar radiation, which was approximately 90 m throughout the whole year). The strong stratification made the bell-shaped SCM more obvious in summer (Figure 5d-3). The SCM began to disappear during the intense winter monsoon reflected by both model and observation (Figure 5d-1).

The modeled seasonal variations in the bacterioplankton and zooplankton concentrations had the same patterns as those of the phytoplankton (Figures 5e and 5f). For example, the surface maximum concentrations of bacterioplankton and zooplankton were 14 mg C m^{-3} and 27 mg C m^{-3} in winter, respectively, and their subsurface maximums of 12 mg C m^{-3} and 25 mg C m^{-3} were located at a depth of about 60 m during warm seasons.

3.2. Responses of the Upper Ocean Ecosystem to Typhoon Damrey

We also examined the modeled physical and biogeochemical responses of the upper ocean ecosystem to Typhoon Damrey. Typhoon Damrey (0518, Category 2, where the category is based on the Saffir-Simpson scale) caused obvious phytoplankton bloom in the SCS and enormous economic loss to Hainan province [*Zheng and Tang*, 2007]. It developed as a tropical depression over the Pacific on 21 September 2005 and moved northwest. On 22 September, it entered the northern part of the SCS, before intensifying to typhoon category and passing through Station A at 12:00 on 24 September. On 25 September, it made landfall on eastern Hainan Island at 18:00 and dissipated over northern Vietnam 3 days later (Figure 1). From the satellite images of SST and surface Chl *a* during the passage of Typhoon Damrey (Figure 6), the typhoon induced an apparent reduction of SST and occurrence of phytoplankton bloom around Station A.

The TYPHOON calculation was performed for Station A, which was under the typhoon's track. The NCEP data showed that the wind speed at Station A started to increase on 22 September, reached a maximum of 20 m s^{-1} on 24 September, and gradually decreased subsequently (Figure 3b).

Modeled results showed that Typhoon Damrey greatly enhanced vertical mixing in the upper ocean (Figure 7a). The modeled surface diffusivity coefficient reached a maximum value of 10^{-1} m^2 s^{-1}, and it was greater than 10^{-4} m^2 s^{-1} in the whole upper 150 m depth on 24 September when the wind speed increased to 20 m s^{-1}. The water was not disturbed by Typhoon Damrey below the 150 m depth.

Modeled vertical profile of the water temperature at Station A on 20 September immediately before the arrival of Typhoon Damrey was in good agreement with the observations reported by *Zheng and Tang* [2007] (Figure 7b). The calculated MLD was approximately 36 m on that day, below which the water was stratified (Figure 7d). Both the modeled and satellite-derived SST data indicated a remarkable decrease with a maximum decrease of ~4.0°C on 24 September (Figure 7e). Figure 7d shows the response of the water temperature to Typhoon Damrey in the upper 150 m depth. The enhanced vertical mixing redistributed the thermal content in the water column. As a consequence, cooling occurred in the upper 50 m and warming occurred from depths of 50 m to 150 m (Figures 7c and 7d). For example, the water temperature at 100 m increased by more than 1.0°C on 24 September (Figure 7e). The MLD deepened remarkably from 36 m to 86 m, but quickly recovered to its original depth, and then gradually deepened following its seasonal variation in October (Figure 7d). Observed vertical profiles of the water temperature during Typhoon Damrey at Station A were not available. The temperature profiles observed in a mooring station on the continental shelf of the northwestern SCS (Station B in Figure 1) indicated that Typhoon Damrey caused a cooling of 4.5°C in the surface layer and a warming of 1.2°C in the subsurface layer (75 m depth) [*Yang et al*., 2015], which were comparable to our results in which the surface temperature decreased by 4.0°C while the water temperature at 75 m depth increased by 1.0°C (Figure 7c).

We also calculated several general nondimensional numbers [*Black and Dickey*, 2008] to make it easier to compare the characteristics of Typhoon Damrey and the responses of physical variables with other studies. The hurricane hazard index was 0.32; the nondimensional storm speed (S) was 1.1; the Burger number (B), indicating the degree of pressure coupling between the mixed layer currents and the thermocline current, was 0.07; the Rossby number for mixed layer current (Q) was 0.05.

Under the influence of Typhoon Damrey, the MLD deepened and exceeded the depth of the nutricline (50 m), thereby resulting in nutrients being enriched in the upper layer. For example, the modeled concentrations of DIN, DIP, and DSi increased sharply at the surface from 0.63, 0.07, and 0.75 mmol m^{-3} to 2.58, 0.17, and 1.81 mmol m^{-3}, respectively, on 24 September. The nutrients in the upper layer then gradually decreased from the maximum because of their consumption by phytoplankton, and their concentrations gradually reached the original values before the arrival of the typhoon.

The simulated surface nutrient and Chl *a* concentrations were low on 20 September before the arrival of Typhoon Damrey (Figures 8 and 9a and 9b). The modeled vertical profile of Chl *a* exhibited the SCM phenomenon with a peak concentration at a depth of ~60 m (Figure 9b). This phenomenon was common in the study area during this season when no episodic disturbances occurred [*Chen*, 2004]. The Chl *a* was distributed uniformly, and the SCM disappeared (Figure 9b) on 24 September. About 1 week after the typhoon, the Chl *a* in the whole euphotic zone increased rapidly in response to the nutrients supplied from the deeper water. As shown in Figures 9a and 9b, the Chl *a* at the surface, subsurface (~60 m), and the depth below the euphotic layer (e.g., 100 m) exhibited different responses to Typhoon Damrey. The modeled surface maximum for the Chl *a* of 0.61 mg m^{-3} appeared on 1 October, which was consistent with the average value of 0.60 mg m^{-3} derived from MODIS and SeaWiFS. In addition to the sea surface, the subsurface (60 m) also exhibited a remarkable Chl *a* increase with a maximum Chl *a* of 0.71 mg m^{-3} on 4 October. At a depth of 100 m, there was also an increase in Chl *a* with a maximum of 0.08 mg m^{-3} on 24 September (Figure 9a). The nutrients in the upper layer were largely consumed after the phytoplankton bloom. The deficiency of nutrients (Figure 8) and grazing by zooplankton (Figure 9d) reduced the Chl *a* (Figures 9a and 9b). After 10 October, the effects of the typhoon were minor. The nutricline and SCM reformed, and they followed their seasonal variations (Figure 9b).

The modeled bacterioplankton and zooplankton (Figures 9c and 9d) exhibited similar responses to the phytoplankton. The subsurface maximums for the bacterioplankton and zooplankton disappeared rapidly on 24 September and then increased, with maxima of 22 mg C m^{-3} for bacterioplankton and 63 mg C m^{-3} for zooplankton in the surface and subsurface layers. The bacterioplankton peaked at the same time as the phytoplankton, but the zooplankton lagged by 3 days.

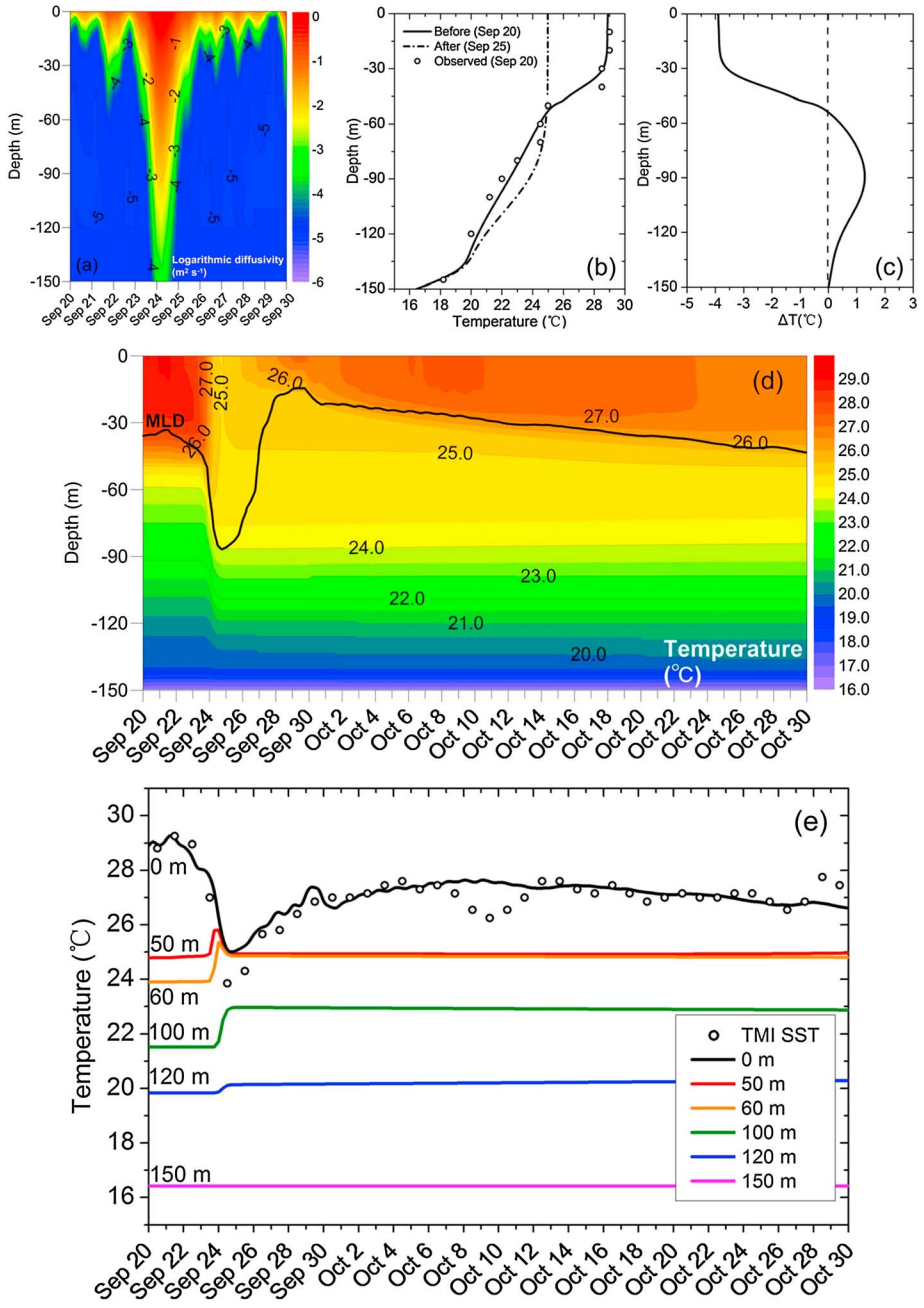

Figure 7. (a) Depth-time plots of the modeled logarithmic distributions of the vertical diffusivity coefficient ($m^2 s^{-1}$) from 20 to 30 September in the TYPHOON simulation. (b) Vertical profiles of the modeled water temperature (°C) pretyphoon (20 September, solid line) and posttyphoon (25 September, dashed line) in the TYPHOON simulation, and observations reported by *Zheng and Tang* [2007] for before the typhoon (20 September, dark circles). (c) The corresponding temperature variation. (d) Depth-time plot of the water temperature (°C) from 20 September to 30 October in the TYPHOON simulation, where the thick solid line represents the mixed layer depth (MLD; unit = m). (e) Time evolution of the water temperature (°C) at depths of 0, 50, 60, 100, 120, and 150 m in the TYPHOON simulation and the satellite sea surface temperature (SST) data acquired by from the TRMM Microwave Imager (TMI, dark circles) from 20 September to 30 October.

3.3. Contributions of Physical and Biogeochemical Processes to the Phytoplankton Biomass in Different Water Layers

Based on satellite and shipboard data, several studies have shown that typhoon-induced vertical mixing can increase the surface Chl *a* [*Zhao et al.*, 2009; *Ye et al.*, 2013; *Zhao et al.*, 2013; *Tang et al.*, 2014]. Given the

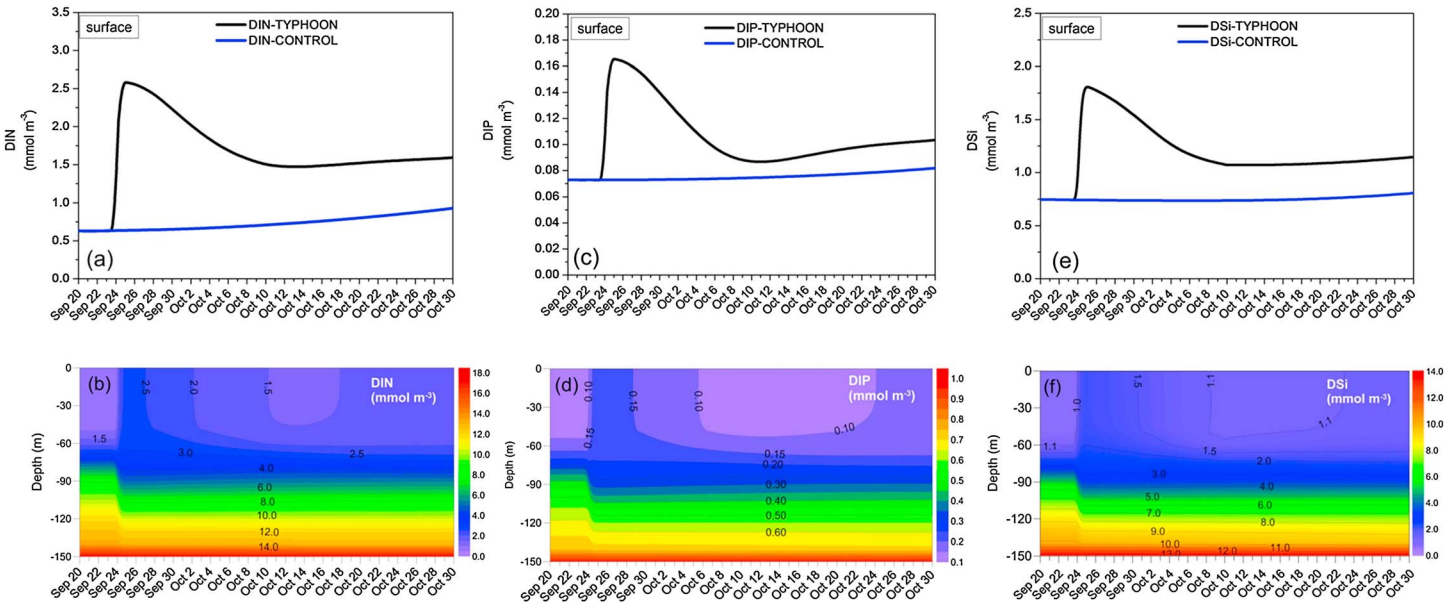

Figure 8. Time series of (a) DIN, (c) DIP, and (e) DSi (mmol m^{-3}) in the surface layer from 20 September to 30 October in the CONTROL (blue line) and TYPHOON (black line) simulations. Depth-time plots of the modeled (b) DIN, (d) DIP, and (f) DSi (mmol m^{-3}) from 20 September to 30 October in the TYPHOON simulation.

existence of the SCM, the increased Chl *a* at the surface is caused partly by mixing subsurface chlorophyll *a* up to the surface, which is referred to as physical process. Strong vertical mixing can also pump nutrients from the deeper water up to the surface layer and promote the growth of phytoplankton, which is referred to as biogeochemical processes. However, it is logistically difficult and expensive to quantify the contributions of these two processes to the increased surface Chl *a* during typhoon events only using observational data.

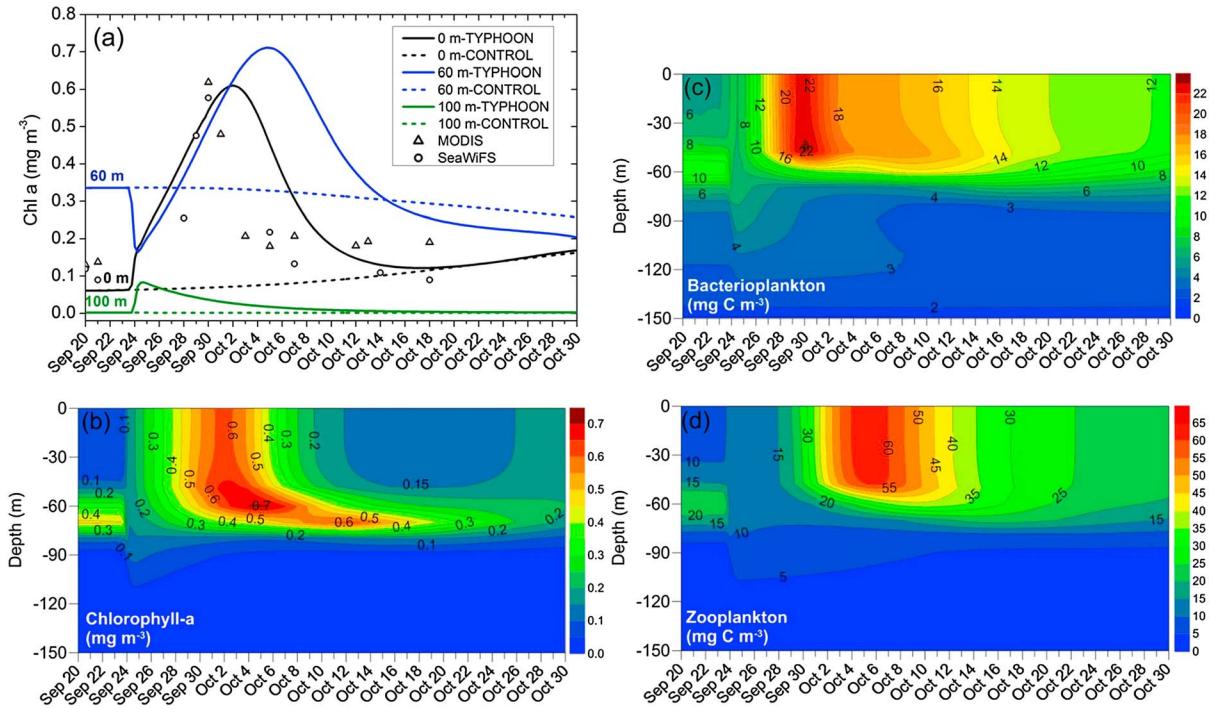

Figure 9. (a) Time series of Chl *a* (mg m^{-3}) in the surface, subsurface, and deep layers from 20 September to 30 October according to the CONTROL (dash line) and TYPHOON (solid line) simulations, and satellite sea surface Chl *a* data acquired from MODIS (dark triangles) and SeaWiFS (dark circles). Depth-time plots of modeled (b) Chl *a*, (c) bacterioplankton (mg C m^{-3}), and (d) zooplankton (mg C m^{-3}) from 20 September to 30 October in the TYPHOON simulation.

Table 4. Contributions of Physical and Biogeochemical Processes to Phytoplankton Biomass Enhancement in Different Water Layers

Water Layer	Stage	Physical Process (mg C m^{-3})	Biogeochemical Processes (mg C m^{-3})
Surface (0 m)	Stage I	1.50	0.27
	Stage II	−12.68	24.54
Subsurface (60 m)	Stage I	−6.42	2.12
	Stage II	−16.78	30.46
100 m		2.46	−0.41

Therefore, we examined our model results to separate the contributions of physical and biogeochemical processes to the phytoplankton biomass in the surface, subsurface, and deeper water layers during the different stages (Table 4). The variation in the phytoplankton biomass is given by the following equation:

$$\frac{\partial P}{\partial t} = \left.\frac{\partial P}{\partial t}\right|_{\text{phys}} + \left.\frac{\partial P}{\partial t}\right|_{\text{bio}}, \tag{3}$$

where the total time rate of change is given by the algebraic sum of a source term due solely to a physical process and by a source/sink term determined by biogeochemical processes. The physical transport term is usually made explicit by using primitive equations of motion in the following form.

$$\left.\frac{\partial P}{\partial t}\right|_{\text{phys}} = \frac{\partial}{\partial z}\left(K_h \frac{\partial P}{\partial z}\right). \tag{4}$$

The description of the processes involved in the biogeochemical dynamics of phytoplankton biomass has the following form.

$$\left.\frac{\partial P}{\partial t}\right|_{2} = \text{Assimilation} - \text{Excretion} - \text{Respiration} - \text{Grazing}. \tag{5}$$

The phytoplankton biomass (P in Figure 10) and its rate of variation caused by physical process ($\left.\frac{\partial P}{\partial t}\right|_{\text{phys}}$ in Figure 10) and biogeochemical processes ($\left.\frac{\partial P}{\partial t}\right|_{\text{bio}}$ in Figure 10) were determined for the surface, subsurface (60 m), and the depth under the euphotic layer, e.g., 100 m.

Figure 10a shows that the typhoon resulted in a maximum increase in the phytoplankton biomass of 13.63 mg C m^{-3} at the surface. The phytoplankton biomass increased gradually after 23 September and reached a maximum of 15.23 mg C m^{-3} on 1 October. The 9 day increasing period was apparently divided into two stages with totally different increases in their slopes, i.e., Stage I from 23 to 24 September with a rapidly increasing slope and Stage II from 24 September to 1 October with a slowly increasing slope. In Stage I, the phytoplankton biomass increased by 1.77 mg C m^{-3} on 24 September. Physical process contributed 1.50 mg C m^{-3}, whereas the contribution of biogeochemical processes was only 0.27 mg C m^{-3}. However, in Stage II, physical process yielded a negative contribution of −12.68 mg C m^{-3}. The contribution of net growth was 24.54 mg C m^{-3}, thereby indicating that the increase in the surface phytoplankton biomass was determined mainly by net growth in Stage II.

Figure 10b shows that the typhoon resulted in a maximum increase in the phytoplankton biomass of 9.38 mg C m^{-3} at a depth of 60 m. The phytoplankton biomass decreased rapidly by 4.32 mg C m^{-3} from 23 to 24 September and then increased to a maximum of 18.0 mg C m^{-3} on 4 October. During the decreasing stage (Stage I), the contributions of physical and biogeochemical processes were −6.42 mg C m^{-3} and 2.12 mg C m^{-3}, respectively. The physical process overwhelmed the biogeochemical processes and caused the disappearance of the SCM. During the increasing stage (Stage II), the phytoplankton biomass exhibited a long-term increase from 24 September to 4 October. The contribution of the physical process remained negative at 16.78 mg C m^{-3}. The biogeochemical contribution of 30.46 mg C m^{-3} led to a net increase in the phytoplankton biomass.

At the depth from the bottom of the euphotic layer to ~150 m (i.e., 100 m in Figure 10c), there was also a small phytoplankton biomass peak on 24 September. The variations due to physical and biogeochemical processes were 2.46 mg C m^{-3} and −0.41 mg C m^{-3}, respectively. The weak increase was caused by downward

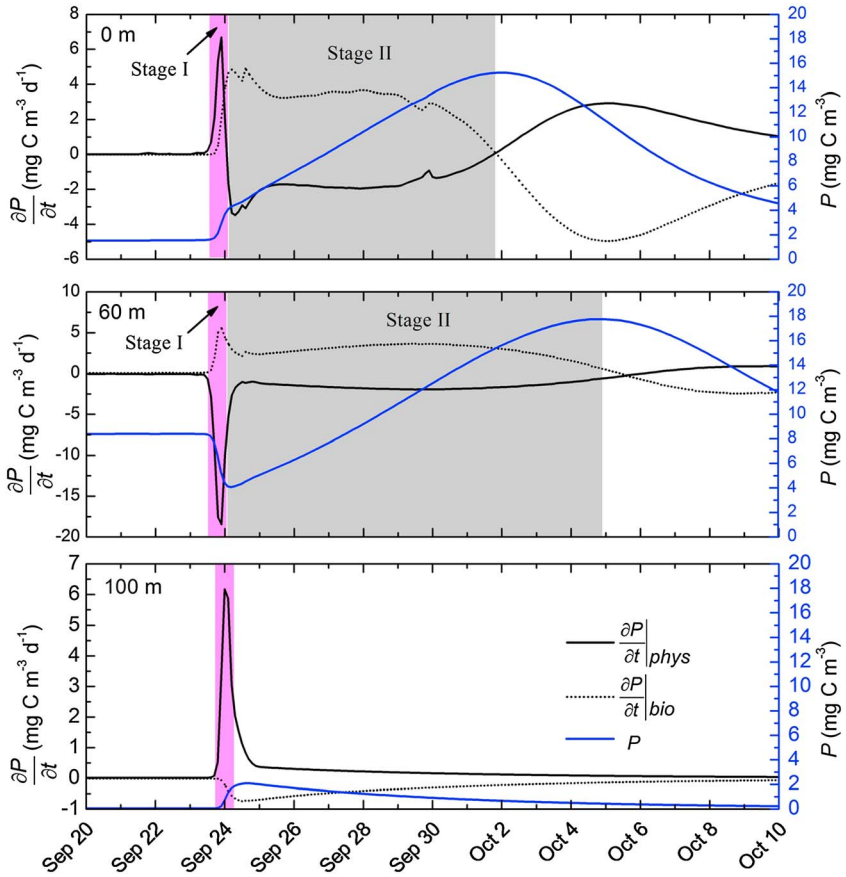

Figure 10. Changing rate of phytoplankton biomass induced by physical (black solid line) and biogeochemical (black dotted line) processes, and the phytoplankton biomass (blue solid line) at depths of (a) 0 m, (b) 60 m, and (c) 100 m from 20 September to 10 October.

entrainment of phytoplankton from the euphotic layer. Subsequently, the phytoplankton biomass decreased due to the domination of death relative to growth.

4. Discussion

4.1. Sensitivity Experiments to Parameters

Sensitivity experiments were carried out to examine how the predicted variables vary with the change of the parameters used in the model (Tables 1 and 2). The predicted state variable in this sensitivity analysis was chosen to be the monthly mean phytoplankton biomass during and 1 month after the passage of the Typhoon Damrey (from 20 September to 20 October). Taking the parameters listed in Tables 1 and 2 as the control run, the value of each selected parameter was increased and decreased by 50% and the model was run for 1 year in each sensitivity experiment. The sensitivity of the predicted state variable to the selected parameter was quantified by a factor $S = \frac{|\Delta F/F|}{|\Delta a/a|}$, where F was the mean phytoplankton biomass from 20 September to 20 October and α was the value of a parameter used in the model. Parameter ΔF was the variation of F corresponding the change ($\Delta\alpha$) of the parameter α.

Fifty-four parameters were tested in this sensitivity analysis (Tables 1 and 2). The sensitivity factor S was smaller than 1.0 for all the parameters and actually less than 0.5 for more than 87% parameters. The predicted variable (mean phytoplankton biomass from 20 September to 20 October) was relatively sensitive to the phytoplankton related parameters, such as the maximum specific photosynthetic rate, half-saturation coefficient for N limitation, excreted fraction of primary production and the characteristic Q_{10} coefficient, and the parameters related to microzooplankton, such as the characteristic Q_{10} coefficient, growth rate, and

assimilation efficiency (Tables 1 and 2: the sensitivity factor *S* was larger than 0.5 for these parameters). The sensitivities to half-saturation coefficient of DIN and DIP were larger than that of DSi, suggesting that the photosynthesis was limited mostly by DIN and occasionally by DIP but never by DSi in our calculations. Besides, the predicted variable was more sensitive to parameters related to microzooplankton rather than to the other two kinds of zooplankton because phytoplankton was mainly grazed by microzooplankton. By changing the parameters within a given range (i.e., 50%), we confirmed that the variations of phytoplankton biomass and the situation of limitation nutrient were relatively stable in our model calculations. Therefore, the model results were likely robust to the model parameters.

4.2. Contributions of Typhoon Damrey to the Supply of Nutrients and the Associated Primary Production

Typhoon Damrey brought cold nutrient-rich deeper water up to the euphotic layer and enhanced primary production. We calculated the net nutrient flux across the euphotic layer depth induced by vertical mixing. The upward transport of DIN, DIP, and DSi increased sharply to maximum values of 182.27 mmol m^{-2} d^{-1}, 8.84 mmol m^{-2} d^{-1}, and 35.85 mmol m^{-2} d^{-1}, respectively, on 24 September, which were nearly 300 times the levels in the CONTROL (0.53 mmol m^{-2} d^{-1}, 0.025 mmol m^{-2} d^{-1}, and 0.69 mmol m^{-2} d^{-1} for DIN, DIP, and Dsi, respectively). The total concentrations supplied during the period from 20 to 30 September were 86.98 mmol m^{-2}, 4.22 mmol m^{-2}, and 67.72 mmol m^{-2} for DIN, DIP, and DSi, respectively, which were more than 100 times those in the CONTROL (5.35 mmol m^{-2}, 0.26 mmol m^{-2}, and 6.82 mmol m^{-2} for DIN, DIP, and DSi, respectively). Among the total annual amounts supplied, these short-term increases caused by Typhoon Damrey contributed 24% of the DIP, 25% of the DIN, and 20% of the DSi. In the southern East China Sea, *Hung et al*. [2013] reported that the DIP and DIN input related to typhoon Morakot (7 to 9 August 2009) accounted for more than 80% of their amounts during the summer; however, no related estimates are available for the SCS.

In our study, we calculated the IPP by integrating the phytoplankton net growth production over the euphotic zone. Based on our CONTROL simulation results and previous observations [*Tseng et al*., 2005], the phytoplankton biomass and primary production in the northern SCS basin were extremely low throughout the whole year. According to the CONTROL simulation, the annual mean value of IPP was 128 mg C m^{-2} d^{-1}. The highest value was 228 mg C m^{-2} d^{-1} in January, and the lowest value was 94 mg C m^{-2} d^{-1} in October. *Tseng et al*. [2005] reported that the IPP at the SEATS station increased to 300 mg C m^{-2} d^{-1} during the winter, but it remained at a low value of ~110 mg C m^{-2} d^{-1} for the rest of the year. *Liu and Chai* [2009] suggested that the mean IPP in the SCS was 196 mg C m^{-2} d^{-1}, with a highest value of 386 mg C m^{-2} d^{-1} in winter and a lowest value of 156 mg C m^{-2} d^{-1} in summer. Thus, our mode results are comparable to those obtained in previous studies.

According to the TYPHOON simulation, the IPP increased to a maximum value of 623 mg C m^{-2} d^{-1} on 1 October, which was more than 6 times than that obtained in the CONTROL simulation (97.78 mg C m^{-2} d^{-1}). The time-integrated IPP from 20 September to 20 October was 9.5×10^3 mg C m^{-2}, which was 2 times higher than the modeled climatological IPP for the same period, where it contributed 14% of the annual-integrated IPP. *Naik et al*. [2008] estimated that a tropical cyclone contributed 5% of the annual total in the Arabian Sea. In the East China Sea, Typhoon Meari induced a threefold IPP increase, which contributed 3.8% of the annual amount [*Siswanto et al*., 2008]. *Lin et al*. [2003] stated that 14 tropical cyclones accounted for 20%–30% of the IPP every year in the SCS. In 2007, Typhoon Hagibis caused a significant phytoplankton bloom, which accounted for 30% of the annual Chl *a* in the middle of the SCS [*Sun et al*., 2010]. A recent study showed that the contribution of typhoons to the annual new production was 5–15% by using the actual typhoons passing through the SCS and considering the intensity of each typhoon during 2003 to 2012 [*Chen et al*., 2015]. The modeled contribution of Typhoon Damrey in our study was comparably high but within the reported range. In fact, our estimation was based on modeled vertical profiles rather than on the satellite-derived values at sea surface, and therefore, it also reflected the increment of production in the subsurface layer. Another factor was that most of the previous studies estimated the contributions of typhoons to the production over the whole SCS or a subregion of SCS, while our study focus on one site (Station A) along the passage of Typhoon Damrey, where the influence of the typhoon was apparently strong.

4.3. Potential Long-Term Influence of Typhoons

Excluding the short-term response, it is not known whether typhoons have any long-term effects. According to the TYPHOON calculation, the mean values of the DIN, DIP, and DSi concentrations in the upper 50 m depth from 1 November until the end of the year (30 December) were 2.0 mmol m^{-3}, 0.13 mmol m^{-3}, and 1.7 mmol m^{-3}, respectively. These values were slightly higher compared with those obtained by the CONTROL simulation (1.6 mmol m^{-3}, 0.12 mmol m^{-3}, and 1.2 mmol m^{-3}, respectively). As a result, the time-integrated IPP from 1 November until the end of the year (30 December) was 1.1×10^4 mg C m^{-2}, i.e., 32% more than that in the CONTROL simulation. Therefore, it may be assumed that typhoons have long-term effects on ocean ecosystems rather than causing a short-term response for several weeks. These findings and hypotheses need to be examined in future studies based on more observations and numerical experiments.

5. Conclusions

In this study, using a 1-D physical-biogeochemical coupled model and previously published observations, we systematically investigated the responses of the upper ocean ecosystem in the basin area of the SCS to Typhoon Damrey. The model reproduced the climatological seasonal variations in the physical and biogeochemical elements based on comparisons of the results obtained by the model and observations collected from WOA2013 at the SEATS station. Observations and our model results demonstrated a remarkable cooling of the SST by ~4.0°C and a maximum increase in the sea surface Chl *a* of ~0.6 mg m^{-3} at Station A, which was under the typhoon track.

The surface Chl *a* increased rapidly from 0.07 to 0.17 mg m^{-3} as the typhoon arrived, and it gradually reached a peak of 0.61 mg m^{-3} after the typhoon's passage. In addition to the surface layer, we considered the responses in the subsurface layer, which is difficult to observe from satellites. The subsurface Chl *a* decreased from 0.34 to 0.17 mg m^{-3} as the typhoon arrived, and it then gradually increased to 0.71 mg m^{-3}. Our analysis of the model results indicated that the initial rapid increase in the surface Chl *a* and the decrease in the subsurface Chl *a* were caused mainly by physical process (vertical mixing), whereas the subsequent gradual increases in Chl *a* in both the surface and subsurface layers were due mainly to biogeochemical processes (net growth of phytoplankton). The gradual increase in the Chl *a* lasted for longer in the subsurface layer than the surface layer.

During the period from 20 September to 20 October, Typhoon Damrey yielded an IPP of 6.5×10^3 mg C m^{-2} accounting for 14% of the annual IPP. This study suggested that typhoon can enhance primary production during its passage and may have potential long-term influence in oligotrophic oceans.

It is widely known that cold SST in the wake of typhoons are caused by the joint effects of upwelling (Ekman pumping) and entrainment (vertical mixing). In this study, we considered entrainment but neglected upwelling because the former is much important than the latter to reduction of SST [*Price*, 1981; *Price et al*., 1994]. Apparently, a three-dimensional model is a better tool to involve more processes associated with typhoons (e.g., wind-driven upwelling). In the near future, we will extend our study to a three-dimensional model and clarify the role of horizontal processes in the response of upper ocean ecosystem to the passage of a typhoon.

Acknowledgments

This research is funded in part by the Chinese Ministry of Science and Technology under contract 2014CB953702, the National Nature Science Foundation of China under contracts 41506013 and 41406010, and the "Strategic Priority Research Program" of the Chinese Academy of Sciences under contract XDA11010101. X. Guo thanks support from JSPS KAKENHI (15H05821). The forcing data of the model were obtained from NCEP reanalysis data sets. The model was validated with the WOA2013 statistical mean data. The daily SST was retrieved from TMI SST datat, and the daily surface Chl *a* were from MODIS-Aqua and SeaWiFS. The other data for this paper is properly cited and referred to in the reference list. We thank Minhan Dai, Zhiyu Liu, and Chuanjun Du from Xiamen University for providing unpublished observations at SEATS station. We thank the Associate Editor and reviewers who provided important and insightful comments that significantly improved the presentation.

References

Ardyna, M., M. Babin, M. Gosselin, and E. Devred (2013), Parameterization of vertical chlorophyll a in the Arctic Ocean: Impact of the subsurface chlorophyll maximum on regional, seasonal and annual primary production estimates, *Biogeosciences*, *10*(6), 4383–4404, doi:10.5194/bg-10-4383-2013.

Babin, S. M., J. A. Carton, T. D. Dickey, and J. D. Wiggert (2004), Satellite evidence of hurricane-induced phytoplankton blooms in an oceanic desert, *J. Geophys. Res.*, *109*, C03043, doi:10.1029/2003JC001938.

Baretta, J. W., W. Ebenhöh, and P. Ruardij (1995), The European regional seas ecosystem model, a complex marine ecosystem model, *Neth. J. SeaRes.*, *33*(3), 233–246.

Bates, N. R., A. H. Knap, and A. F. Michaels (1998), Contribution of hurricanes to local and global estimates of air-sea exchange of CO_2, *Nature*, *395*(6697), 58–61.

Black, W. J., and T. D. Dickey (2008), Observations and analyses of upper ocean responses to tropical storms and hurricanes in the vicinity of Bermuda, *J. Geophys. Res.*, *113*, C08009, doi:10.1029/2007JC004358.

Blumberg, A. F., and G. L. Mellor (1987), A description of a three-dimensional coastal ocean circulation model, *Three-Dimensional Coastal Ocean Models*, edited by N. S. Heaps, 1–16, AGU, Washington, D. C., doi:10.1029/CO004p0001.

Chen, X. Y., D. L. Pan, Y. Bai, X. Q. He, C. A. Chen, Y. Kang, and B. Y. Tao (2015), Estimation of typhoon-enhanced primary production in the South China Sea: A comparison with the western north pacific, *Cont. Shelf Res.*, *111*(1), 296–306, doi:10.1016/j.csr.2015.10.003.

Chen, Y. J. (2004), Estimation of primary production in the South China Sea and observation of particulate organic matter at SEATS station: Application in the validation and improvement of the coupled physical-biogeochemical model of South China Sea [in Chinese with English abstract], pp. 1–109, National Taiwan Univ.

Cione, J. J., and E. W. Uhlhorn (2003), Sea surface temperature variability in hurricanes: Implications with repect to intensity change, *Mon. Weather Rev.*, *131*, 1783–1796.

Cullen, J. J., and R. W. Eppley (1981), Chlorophyll maximum layers of the Southern-California Bight and possible mechanisms of their formation and maintenance, *Oceanol. Acta*, *4*(1), 23–32.

Dickey, T., D. Frye, J. McNeil, D. Manov, N. Nelson, D. Sigurdson, H. Jannasch, D. Siegel, T. Michaels, and R. Johnson (1998), Upper-ocean temperature response to Hurricane Felix as measured by the Bermuda Testbed Mooring, *Mon. Weather Rev.*, *126*, 1195–1201.

Fairall, C. W., E. F. Bradley, D. P. Rogers, J. B. Edson, and G. S. Young (1996), Bulk parameterization of air-sea fluxes for Tropical Ocean-Global Atmosphere Coupled-Ocean Atmosphere Response Experiment, *J. Geophys. Res.*, *101*, 3747–3764, doi:10.1029/95JC03205.

Fisher, T. R. (1992), Nutrient limitation of phytoplankton in Chesapeake Bay, *Mar. Ecol. Prog. Ser.*, *82*(1), 51–63.

Gong, G., F. Shiah, K. Liu, Y. Wen, and M. Liang (2000), Spatial and temporal variation of chlorophyll-a, primary productivity and chemical hydrography in the southern East China Sea, *Cont. Shelf Res.*, *20*, 411–436, doi:10.1016/S0278-4343(99)00079-5.

Gong, X., J. Shi, H. W. Gao, and X. H. Yao (2015), Steady-state solutions for subsurface chlorophyll maximum in stratified water columns with a bell-shape vertical profile of chlorophyll, *Biogeosciences*, *12*(6), 905–919, doi:10.5194/bg-12-905-2015.

Guan, S., W. Zhao, J. Huthnance, J. Tian, and J. Wang (2014), Observed upper ocean response to typhoon Megi (2010) in the northern South China Sea, *J. Geophys. Res. Oceans*, *119*, 3134–3157, doi:10.1002/2013JC009661.

Ha, Y., Z. Zhong, Y. Sun, and W. Lu (2014), Decadal change of South China Sea tropical cyclone activity in mid-1990s and its possible linkage with intraseasonal variability, *J. Geophys. Res. Atmos.*, *119*, 5331–5344, doi:10.1002/2013JD021286.

Han, G., Z. Ma, and N. Chen (2012), Hurricane Igor impacts on the stratification and phytoplankton bloom over the Grand Bankss, *J. Mar. Syst.*, *100–101*, 19–25, doi:10.1016/j.jmarsys.2012.03.012.

Hu, H. G., Y. L. Yuan, and Z. W. Wan (2004), Study on hydrodynamic environment of the Bohai Sea, the Huanghai Sea and the East China Sea with wave-current coupled numerical model [in Chinese with English abstract], *Acta Oceanol. Sin.*, *26*, 19–32.

Huang, C. J., and F. Qiao (2010), Wave-turbulence interaction and its induced mixing in the upper ocean, *J. Geophys. Res.*, *115*, C04026, doi:10.1029/2009JC005853.

Huang, C. J., F. Qiao, Z. Song, and T. Ezer (2011), Improving simulations of the upper ocean by inclusion of surface waves in the Mellor-Yamada turbulence scheme, *J. Geophys. Res.*, *116*, C01007, doi:10.1029/2010JC006320.

Hung, C., C. Chung, G. Gong, S. Jan, Y. Tsai, K. Chen, W. C. Chou, M. Lee, Y. Chang, and M. Chen (2013), Nutrient supply in the southern East China Sea after typhoon Morakot, *J. Mar. Res.*, *71*, 133–150, doi:10.1357/002224013807343425.

Jacob, S. D., L. K. Shay, A. J. Mariano, and P. G. Black (2000), The 3D oceanic mixed layer response to Hurricane Gilbert, *J. Phys. Oceanogr.*, *30*(6), 1407–1429.

Knaff, J. A., M. Demaria, C. R. Sampson, J. E. Peak, J. Cummings, and W. H. Schubert (2013), Upper oceanic energy response to tropical cyclone passage, *J. Clim.*, *26*(8), 2631–2650, doi:10.1175/JCLI-D-12-00038.1.

Li, R. C., and W. Zhou (2014), Interdecadal change in South China Sea tropical cyclone frequency in association with zonal sea surface temperature gradient, *J. Clim.*, *27*, 5468–5480, doi:10.1175/JCLI-D-13-00744.1.

Lin, I., W. T. Liu, C. C. Wu, G. T. Wong, C. Hu, Z. Chen, W. D. Liang, Y. Yang, and K. K. Liu (2003), New evidence for enhanced ocean primary production triggered by tropical cyclone, *Geophys. Res. Lett.*, *30*(13), 1718, doi:10.1029/2003GL017141.

Liu, G., and F. Chai (2009), Seasonal and interannual variability of primary and export production in the South China Sea: A three-dimensional physical-biogeochemical model studyy, *ICES J. Mar. Sci.*, *66*, 420–431, doi:10.1093/icesjms/fsn219.

Liu, K. K., Y. J. Chen, C. M. Tseng, I. I. Lin, H. B. Liu, and A. Snidvongs (2007), The significance of phytoplankton photo-adaptation and benthic-pelagic coupling to primary production in the south china sea: Observations and numerical investigations, *Deep Sea Res.*, *54*(14), 1546–1574, doi:10.1016/j.dsr2.2007.05.009.

Liu, K., S. Chao, P. Shaw, G. Gong, C. Chen, and T. Y. Tang (2002), Monsoon-forced chlorophyll distribution and primary production in the South China Sea: Observations and a numerical study, *Deep Sea Res., Part I*, *49*(8), 1387–1412, doi:10.1016/S0967-0637(02)00035-3.

Liu, K., L. Wang, M. Dai, C. Tseng, Y. Yang, C. Sui, L. Oey, K. Tseng, and S. Huang (2013), Inter-annual variation of chlorophyll in the northern South China Sea observed at the SEATS Station and its asymmetric responses to climate oscillation, *Biogeosciences*, *10*, 7449–7462, doi:10.5194/bg-10-7449-2013.

Martin, P. J. (1985), Simulation of the mixed layer at OWS November and Papa with several models, *J. Geophys. Res.*, *90*, 903–916, doi:10.1029/JC090iC01p00903.

Naik, H., S. Naqvi, T. Suresh, and P. V. Narvekar (2008), Impact of a tropical cyclone on biogeochemistry of the central Arabian Sea, *Global Biogeochem. Cycles*, *22*, GB3020, doi:10.1029/2007GB003028.

Price, J. E., J. B. Sanford, and G. Z. Forristall (1994), Forced stage response to a moving hurrican, *J. Phys. Oceanogr.*, *24*(2), 233–260.

Price, J. F. (1981), Upper ocean response to a hurricane, *J. Phys. Oceanogr.*, *11*(2), 153–175.

Raimbault, P., B. Coste, M. Boulhadid, and B. Boudjellal (1993), Origin of high phytoplankton concentration in deep chlorophyll maximum (DCM) in a frontal region of the Southwestern Mediterranean Sea (Algerian Current), *Deep Sea Res., Part I*, *40*(4), 791–804.

Shan, H., Y. Guan, and J. Huang (2014), Investigating different bio-responses of the upper ocean to Typhoon Haitang using Argo and satellite data, *Chinese Sci. Bull.*, *59*(8), 785–794, doi:10.1007/s11434-013-0101-9.

Shibano, R., Y. Yamanaka, N. Okada, T. Chuda, S. I. Suzuki, H. Niino, and M. Toratani (2011), Responses of marine ecosystem to typhoon passages in the western subtropical North Pacific, *Geophys. Res. Lett.*, *38*, L18608, doi:10.1029/2011GL048717.

Siswanto, E., J. Ishizaka, A. Morimoto, K. Tanaka, K. Okamura, A. Kristijono, and T. Saino (2008), Ocean physical and biogeochemical responses to the passage of Typhoon Meari in the East China Sea observed from Argo float and multiplatform satellites, *Geophys. Res. Lett.*, *35*, L15604, doi:10.1029/2008GL035040.

Sun, L., Y. Yang, T. Xian, Z. Lu, and Y. Fu (2010), Strong enhancement of chlorophyll a concentration by a weak typhoon, *Mar. Ecol.Prog. Ser.*, *404*, 39–50, doi:10.3354/Meps08477.

Tang, D. L., H. Kawamura, H. Doan Nhu, and W. Takahashi (2004a), Remote sensing oceanography of a harmful algal bloom off the coast of southeastern Vietnam, *J. Geophys. Res.*, *109*, C03014, doi:10.1029/2003JC002045.

Tang, D. L., H. Kawamura, T. Van Dien, and M. Lee (2004b), Offshore phytoplankton biomass increase and its oceanographic causes in the South China Sea, *Mar. Ecol. Prog. Ser.*, *268*, 31–41.

Tang, D. L., G. Sui, G. Lavy, D. Pozdnyakov, Y. T. Song, and A. D. Switzer (2014), *Typhoon Impact and Crisis Management*, Springer, Berlin Heidelberg, doi:10.1007/978-3-642-40695-9.

Tseng, C. M., G. T. Wong, I. I. Lin, C. R. Wu, and K. K. Liu (2005), A unique seasonal pattern in phytoplankton biomass in low-latitude waters in the South China Sea, *Geophys. Res. Lett.*, *32*, L08608, doi:10.1029/2004GL022111.

Vichi, M., J. W. Baretta, J. G. Baretta-Bekker, W. Ebenhoh, C. Kohlmeier, P. Ruardij, N. Pinardi, and M. Zavatarelli (2004), European Regional Seas Ecosystem Model III, Review of the biogeochemical equations, Documentation Release Version: 3.4-alpha.

Wagner, R. G. (1997), Decadal-scale trends in mechanisms controlling meridional sea surface temperature gradients in the tropical Atlantic, *J. Geophys. Res.*, *101*, 16,683–16,694, doi:10.1029/96JC01214.

Walker, N. D., R. R. Leben, and S. Balasubramanian (2005), Hurricane-forced upwelling and chlorophyll a enhancement within cold-core cyclones in the Gulf of Mexico, *Geophys. Res. Lett.*, *32*, L18610, doi:10.1029/2005GL023716.

Wang, G., Z. Ling, and C. Wang (2009), Influence of tropical cyclones on seasonal ocean circulation in the South China Sea, *J. Geophys. Res.*, *114*, C10022, doi:10.1029/2009JC005302.

Wang, G., J. Su, Y. Ding, and D. Chen (2007), Tropical cyclone genesis over the South China Sea, *J. Mar. Syst.*, *68*(3), 318–326, doi:10.1016/j.jmarsys.2006.12.002.

Wong, G. T., T. Ku, M. Mulholland, C. Tseng, and D. Wang (2007), The SouthEast Asian time-series study (SEATS) and the biogeochemistry of the South China Sea—An overview, *Deep Sea Res., Part II*, *54*, 1434–1447, doi:10.1016/j.dsr2.2007.05.012.

Yang, B., Y. Hou, P. Hu, Z. Liu, and Y. Liu (2015), Shallow ocean response to tropical cyclones observed on the continental shelf of the northwestern South China Sea, *J. Geophys. Res. Oceans*, *120*, 3817–3836, doi:10.1002/2015JC010783.

Yang, H., Q. Liu, Z. Liu, D. Wang, and X. Liu (2002), A general circulation model study of the dynamics of the upper ocean circulation of the South China Sea, *J. Geophys. Res.*, *107*(C7), 3085, doi:10.1029/2001JC001084.

Ye, H. J., Y. Sui, D. L. Tang, and Y. D. Afanasyev (2013), A subsurface chlorophyll a bloom induced by typhoon in the South China Sea, *J. Mar. Syst.*, *128*, 138–145, doi:10.1016/j.jmarsys.2013.04.010.

Zedler, S. E., T. D. Dickey, S. C. Doney, J. F. Price, X. Yu, and G. L. Mellor (2002), Analyses and simulations of the upper ocean's response to Hurricane Felix at the Bermuda Testbed Mooring site: 13–23 August 1995, *J. Geophys. Res.*, *107*(C12), 3232, doi:10.1029/2001JC000969.

Zhang, S. W. (2003), Effect mechanisms on chlorophyll-a vertical distribution in the summer within Yellow Sea Cold Water Mass [in Chinese with English abstract], *Oceanologia Et Limnologia Sinica*, *2*, 7.

Zhang, S., L. Xie, Y. Hou, H. Zhao, Y. Qi, and X. Yi (2014), Tropical storm-induced turbulent mixing and chlorophyll-a enhancement in the continental shelf southeast of Hainan Island, *J. Mar. Syst.*, *129*, 405–414.

Zhao, H., D. Tang, and Y. Wang (2008), Comparison of phytoplankton blooms triggered by two typhoons with different intensities and translation speeds in the South China Sea, *Mar. Ecol. Prog. Ser.*, *365*, 57–65, doi:10.3354/meps07488.

Zhao, H., D. Tang, and D. Wang (2009), Phytoplankton blooms near the Pearl River estuary induced by Typhoon Nuri, *J. Geophys. Res.*, *114*, C12027, doi:10.1029/2009JC005384.

Zhao, H., G. Han, S. Zhang, and D. Wang (2013), Two phytoplankton blooms near Luzon Strait generated by lingering Typhoon Parma, *J. Geophys. Res. Biogeosci.*, *118*, 412–421, doi:10.1002/jgrg.20041.

Zhao, H., J. Shao, G. Han, D. Yang, and J. Lv (2015), Influence of typhoon Matsa on phytoplankton chlorophyll-a off East China, *PLoS One*, *10*(9), 1–13, e0137863, doi:10.1371/journal.pone.0137863.

Zheng, G. M., and D. Tang (2007), Offshore and nearshore chlorophyll increases induced by typhoon winds and subsequent terrestrial rainwater runoff, *Mar. Ecol. Prog. Ser.*, *333*, 61–74, doi:10.3354/meps333061.